

3. TIMING CALIBRATION METHODS AND VALIDATION

In this chapter we go into detail about the calibration procedure and the performance of the Electromagnetic Calorimeter Timing System (EMTiming) and the Central Outer Tracker (COT) systems for use in the final photon timing measurement, t_{corr} . We use $W \rightarrow e\nu \rightarrow e + \cancel{E}_T$ events corresponding to the same data taking period as the exclusive $\gamma + \cancel{E}_T$ data set. These $e + \cancel{E}_T$ events have the particular advantage of mimicking the $\gamma + \cancel{E}_T$ final state if we simply ignore the track from the electron when performing the vertexing but use it to help identify the correct vertex location. As we will see, the combination of timing systems have a combined resolution of 0.65 ns for events well matched to the vertex and that after calibrations the EMTiming and COT systems show no systematic variations as a function of all the important event observables to less than <100 ps.

We begin by laying out the tolerances needed for the timing calibrations as well as the procedure that will be followed in order to achieve those tolerances. From there we describe the data selection requirements as well as give more detail on the reasoning behind selecting this subset of events. Next we go into detail about the various calibration distributions and procedures for the tracks from the COT, for vertices constructed using tracks from the COT, and finally for the EMTiming system used in combination with the tracking. Lastly, we present results that demonstrate that the system is well calibrated and has systematic variations that are small compared to the needed tolerances.

Before proceeding, we note that the set of precision calibrations described below are performed after a preliminary calibration has already been done on both the COT and EMTiming systems. These calibrations on the COT and EMTiming data are discussed in detail in Reference [71], of which we give two examples here. Specifically, for the EMTiming system, a preliminary calibration takes into account the time required for the PMT signal to travel to the TDC, an energy-dependent

(slewing) correction due to the use of fixed-height discriminators, and a correction that takes into account the energy difference deposited in the two PMTs. This set of calibrations to the EMTiming system is described in greater detail in Reference [52] and is determined from fits for each channel using high statistics jet data samples. This calibration is done tower-by-tower and combined for various run sections, but only is done relative to the mean time and collision position of the sample used to select events. Since the mean time and position can vary from tower to tower this means that the calibrations can be off by almost a nanosecond which is outside our tolerance window. Additionally, run-by-run variations within a run section can vary by a full nanosecond.

Similarly, for the COT, a preliminary timing calibration is done between runs and is described in more detail in Reference [72]. In this procedure an injected calibration pulse sends a signal to each TDC similar to how real data is read out from the detector. The start time for each channel is read out and the channel-to-channel offsets are calculated and averaged before being subtracted off. These offsets are used to correct the raw hit times that come from the COT. This calibration removes channel-to-channel differences in the readout time of the COT that may arise because of variance among the electronics associated with the readout or because of differences in the cable lengths from the COT. We next move to our procedure which has a more rigorous methodology and uses improved resolutions and multiple iterations to finely tune the calibrations.

3.1 Calibration Tolerances Determination

Accurate measurement and understanding of the performance of the various timing systems used in the delayed photon analysis is of the utmost importance in identifying any evidence for new physics using the variable t_{corr} as defined in Equation 1.8. Figure 3.1 shows an example of how a systematic bias in the measurement of the wrong vertex events could result in a shift of the mean of the wrong vertex dis-

tribution. This bias could lead to an “artificial excess” of events in the signal region and may be misidentified as evidence for new physics. Such an excess could appear if there is a systematic shift present in one system but not present in the other that would get subtracted off if the right vertex were selected, but not if a wrong vertex is selected. For example, an artificial shift in the arrival time (t_f as measured using the EMTiming time) that is not corrected for when selecting an incorrect initial time (vertex time) can lead to a bias in the resulting corrected time (t_{corr}). This bias would tend to show up in the wrong vertex distribution since any artificial shift in the timing systems would be exasperated by the fact that a random initial time was chosen from the wrong vertex.

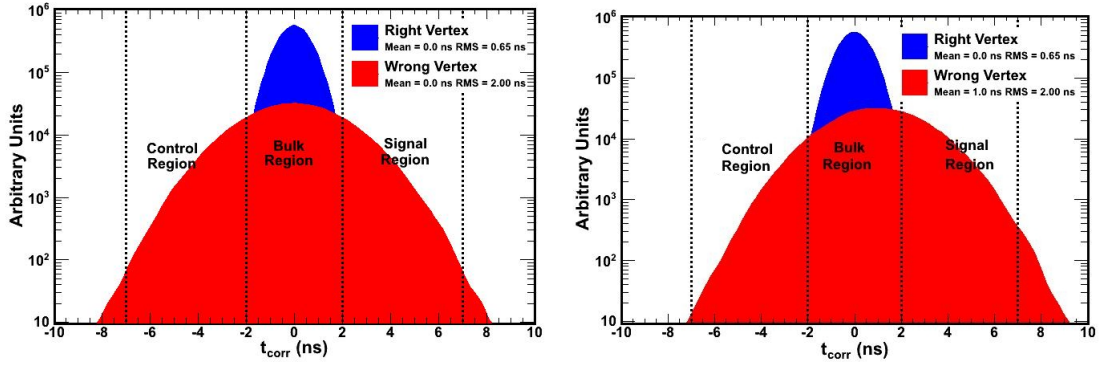


Fig. 3.1. Monte Carlo simulation of a shift in the mean of our wrong vertex timing distribution that can cause an excess in the ratio of the number of events in the signal region ($2 \text{ ns} < t_{corr} < 7 \text{ ns}$) to number of events in the control region ($-7 \text{ ns} < t_{corr} < -2 \text{ ns}$).

Figure 3.2 quantifies how a large timing shift in the measurement of t_{corr}^{WV} translates into a potential excess in the number of large time events using a straightforward calculation. To understand the calculation quantitatively, we start with the assumption that the wrong vertex timing distribution is given by a Gaussian with a mean of μ and an RMS of 2.0 ns and we can integrate the probability for a sample of events

to show up in the control region ($-7 \text{ ns} < t_{corr} < -2 \text{ ns}$) and in the signal region ($2 \text{ ns} < t_{corr} < 7 \text{ ns}$).

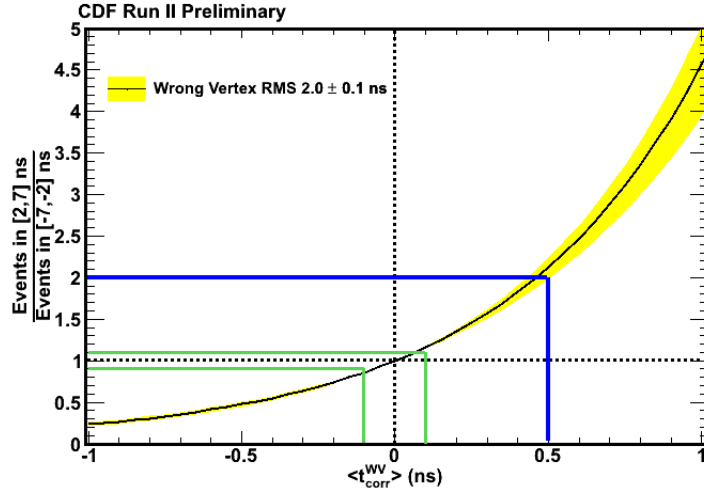


Fig. 3.2. A calculation of how a shift in the mean of the wrong vertex timing distribution, $\langle t_{corr}^{WV} \rangle$, can change the ratio of the number of events in the timing region $2 \text{ ns} < t_{corr} < 7 \text{ ns}$ (Signal Region) to number of events in the timing region $-7 \text{ ns} < t_{corr} < -2 \text{ ns}$ (Control Region) for a sample of SM collision events. The nominal ratio of one for a wrong vertex mean of 0.0 ns shown by the dashed black line. The blue line demonstrates that a value of $\langle t_{corr}^{WV} \rangle = 0.5$ gives you twice as many events in the signal region from SM sources than in the control region. The solid green lines indicate the desired tolerance, 100 ps , on systematic variations in $\langle t_{corr}^{WV} \rangle$. This tolerance was chosen because a shift of 100 ps $\langle t_{corr}^{WV} \rangle$ has less than a 10% effect in terms of an artificial “excess” or “deficit” of events expected in the signal region.

Spelling it out in more detail, we can describe the number of events in any region, illustrated in Figure 3.1, as having two components. Namely, the number of events coming from the right vertex (N_{RV}) and the number of events coming from the wrong vertex (N_{WV}). For clarity we take the number of events in the control region (ignoring the cosmics background for the moment), ($N_{Control}$) and write:

$$N_{Control} = \beta_{RV}^{[-7,-2]ns} \cdot N_{RV} + \beta_{WV}^{[-7,-2]ns} \cdot N_{WV} \quad (3.1)$$

where $\beta_{RV}^{[-7,-2]ns}$ and $\beta_{WV}^{[-7,-2]ns}$ can be thought of the fraction of right vertex and wrong vertex events in this region. Because the distributions are well described by Gaussians, shown in more detail in Chapter 5, $\beta_{RV}^{[-7,-2]ns}$ and $\beta_{WV}^{[-7,-2]ns}$ are given by the error function (*Erf*, [73]) of the right vertex and wrong vertex Gaussians and are hence a function of the mean and RMS of those Gaussians. The error function gives the integrated probability, assuming normally distributed errors with standard deviation σ , having a distance less than some value from the mean of the distribution [73]. The error function is generically defined as

$$Erf(x) = \frac{2}{\pi} \int_0^x e^{-t^2} dt. \quad (3.2)$$

Thus for $\beta_{RV}^{[-7,-2]ns}$, since we know the mean and RMS of the right vertex Gaussian distribution we can write:

$$\beta_{RV}^{[-7,-2]ns} = Erf\left(\frac{\sigma_{[0,-2]ns}^{RV}}{2}\right) - Erf\left(\frac{\sigma_{[0,-7]ns}^{RV}}{2}\right) \quad (3.3)$$

where $\sigma_{[x,y]ns}^{RV}$ describes the distance from the mean value in terms of multiples of the RMS where the factor of $\frac{1}{2}$ in Equation 3.3 comes from the fact we are only integrating one side of the Gaussian. For example, $\sigma_{[0,-2]ns}^{RV}$ is the distance from 0 ns to -2 ns in multiples of the right vertex RMS. Namely, $\frac{2ns}{0.65ns} = 3.08$ which is then put into Equation 3.3 where we are evaluating this error function for the right vertex at two points (-2 ns and -7 ns) assuming the mean of the distribution is at 0 ns. Specifically this implies:

$$\begin{aligned} \sigma_{[\mu,x]ns}^{RV} &= \frac{x-\mu}{\sigma^{RV}\sqrt{2}} \\ \sigma_{[0,-2]ns}^{RV} &= \frac{2}{0.65\sqrt{2}} \end{aligned} \quad (3.4)$$

where σ^{RV} is the RMS of the right vertex (0.65 ns) and we have taken $\mu = 0$. Analogously we evaluate the second error function $Erf(\frac{\sigma^{RV}}{2})$ in the same way thus giving us the fraction of events we expect from the right vertex in the control region.

Similarly we evaluate $\beta_{WV}^{[-7,-2]ns}$ which is the fraction of events from the wrong vertex Gaussian in the control region.

$$\beta_{WV}^{[-7,-2]ns}(\mu) = Erf(\frac{\sigma^{WV}}{2}) - Erf(\frac{\sigma_{[\mu,-7]ns}^{WV}}{2}) \quad (3.5)$$

where

$$\begin{aligned} \sigma_{[\mu,x]ns}^{WV} &= \frac{x-\mu}{\sigma^{WV}\sqrt{2}} \\ \sigma_{[\mu,-2]ns}^{WV} &= \frac{2-\mu}{2.0\sqrt{2}} \\ \sigma_{[\mu,-7]ns}^{WV} &= \frac{7-\mu}{2.0\sqrt{2}} \end{aligned} \quad (3.6)$$

where in Equations 3.6 we explicitly leave the mean of the wrong vertex as a variable allowing us to evaluate this for a range of different wrong vertex means with an RMS = 2.0 ns. Thus, we have reduced Equation 3.1 to having only three unknowns, namely N_{RV} , N_{WV} , and μ . We now note that we can write a very similar equation for the number of events in the bulk region (-2 ns to 2 ns):

$$N_{Bulk} = \beta_{RV}^{[-2,2]ns} \cdot N_{RV} + \beta_{WV}^{[-2,2]ns} \cdot N_{WV} \quad (3.7)$$

where $\beta_{RV}^{[-2,2]ns}$ and $\beta_{WV}^{[-2,2]ns}$ are the fraction of right vertex and wrong vertex in the bulk region. Again, we write the error functions of the right vertex and wrong vertex Gaussians in this region as:

$$\begin{aligned} \beta_{RV}^{[-2,2]ns} &= Erf(\frac{\sigma^{RV}}{2}) - Erf(\frac{\sigma_{[2,0]ns}^{RV}}{2}) \\ \beta_{WV}^{[-2,2]ns} &= Erf(\frac{\sigma_{[\mu,-2]ns}^{WV}}{2}) - Erf(\frac{\sigma_{[2,\mu]ns}^{WV}}{2}). \end{aligned} \quad (3.8)$$

The evaluation of the error functions in Equation 3.8 follows exactly as before. Since we can count the number of events in both regions straightforwardly, after

subtracting off cosmics in the data, we are left with Equations 3.1 and 3.7 giving two equations and three unknowns. Said differently, we can exactly solve for the number of events in any timing region, in particular the signal region, in terms of the number of events from the right vertex and wrong vertex Gaussians if we can measure, or assume μ . Moreover, we can solve this for a range of wrong vertex means as well as allowing the wrong vertex RMS to vary within known systematics.

Looking at the ratio of the $\frac{N_{SR}}{N_{CR}}$ has the advantage of the normalization of the Gaussians dropping out of the prediction in the limit that the contribution from $\beta_{RV} \cdot N_{RV}$ is small. Doing all the steps we find that the only important variable is the mean of the wrong vertex distribution using

$$Ratio(\mu) = \frac{N_{Signal}}{N_{Control}}(\mu) = \frac{\beta_{RV}^{[2,7]ns} \cdot N_{RV} + \beta_{WV}^{[2,7]ns} \cdot N_{WV}}{\beta_{RV}^{[-7,-2]ns} \cdot N_{RV} + \beta_{WV}^{[-7,-2]ns} \cdot N_{WV}} \quad (3.9)$$

where, if we assume the contribution from β_{RV} is small we find

$$\begin{aligned} Ratio(\mu) &\sim \frac{\beta_{WV}^{[2,7]ns} \cdot N_{WV}}{\beta_{WV}^{[-7,-2]ns} \cdot N_{WV}} \\ Ratio(\mu) &\sim \frac{\beta_{WV}^{[2,7]ns}}{\beta_{WV}^{[-7,-2]ns}} \end{aligned} \quad (3.10)$$

Thus, to a good degree of approximation, we can estimate the ratio as a function of the wrong vertex mean, $Ratio(\mu)$ which is the black curve in Figure 3.2 (the yellow band corresponds to an uncertainty on the RMS of the wrong vertex mean of 5%, where this uncertainty is determined using the methods in Chapter 5). Said differently, given a number of events in the control region and the mean of the wrong vertex we can predict the number of events in the signal region coming from wrong vertex sources using the relationship

$$N_{Signal} = R(\mu) \cdot N_{Control} \quad (3.11)$$

Coming back to Figure 3.2, we see that a timing shift of ≈ 500 ps in the wrong vertex distribution (dashed blue line) can lead to twice as many events in the signal region than would be found in the control region from SM sources. Previous versions of this analysis assumed $\mu = \langle t_{corr}^{WV} \rangle = 0$ ns which gives us back the original assumption of $N_{Signal} = N_{Control}$. More so, Figure 3.2 allows us to understand what the tolerance for calibrations on the t_{corr} variable should be, specifically as shown by the solid green lines which indicate that variations of less than 100 ps (0.1 ns) have a negligible effect ($< 10\%$) in terms of creating an artificial “excess” or “deficit” of events expected in the signal region. With this knowledge, we are able to lay out a general procedure for calibrating the various timing subsystems that go into the t_{corr} variable.

In the next section we describe the selection of electron events from $W \rightarrow e\nu$ data as well as the broad overall calibration procedure. This procedure includes the calibration of COT tracks, SpaceTime vertices, and the EMTiming system. It is worthwhile to mention that a well “calibrated” system is one where the mean of the t_{corr} distribution for right vertex events is centered at $t_{corr} = 0$ ns, and that this distribution does not show any systematic variation as a function of any important variables in the analysis. To “calibrate” the system is to add corrections to t_0 for the tracking and t_f for the EMTiming system such that each system does not have systematic variations as a function of any important measurement variable. Often this is an offset. For example, if we note that all the events from a certain run have a mean track $t_0 = -1$ ns, then we add 1 ns to all events in that run. Since there are correlations between variables we will also have correlated corrections we often need to iterate the calibration procedure until the samples stabilize in terms of the magnitude of the corrections being generated. We stop when all the means and variations are small compared to our tolerances. Additionally, we check to be sure that the distributions are well centered and symmetric.

3.1.1 Outline of the Calibration Procedure

We begin this section by selecting a set of events in data which pass the $W \rightarrow e\nu \rightarrow e + \cancel{E}_T$ requirements described below and summarized in Table 3.1. We next describe the matching criteria and how they were selected.

Event Selection	Number of Events
Pass Trigger and Good Run List requirements <i>See Table 2.2 and 2.3 and Section 2.4</i>	4,858,466
$\cancel{E}_T^0 > 30 \text{ GeV}$	3,893,252
Identified Electron w/ $E_T^0 > 30 \text{ GeV}$ <i>(See Table 2.9)</i>	3,221,638
Passing Beam Halo Rejection <i>(Discussed in detail later)</i>	3,184,983
Good Space Time Vertex <i>Note: Electron Track is removed from the Vertexing</i> <i>See Table 2.10</i>	2,605,338
Only one SpaceTime Vertex is matched to the electron track $ \Delta T = t_{electron} - t_0 < 1.8 \text{ ns}$ and $ \Delta Z = z_{electron} - z_0 < 3.0 \text{ cm}$	2,010,699

Table 3.1

Event reduction table summarizing the requirements used to generate the $e + \cancel{E}_T$ timing calibration sample. Note that the final number of events reported here is after all calibrations have been applied.

A sample of electrons from $W \rightarrow e\nu$ events are chosen to calibrate the detector systems as they do an excellent job providing a pure sample of electrons. These events mimick the way a photon interacts with the calorimeter as well as directly identifying the origin of the event in both space and time. This allows us to correctly calibrate the timing systems to this origin event-by-event. To ensure that the electron comes from the vertex we are considering, we require that the electron track has the same value of z_0 and t_0 as the primary vertex within some reasonable tolerances. Figure 3.3

shows the typical matching quality variables by which we match the electron track to the vertex as they appear before our precision timing calibrations. Here, ΔT is the difference between the reported track time and the vertex time ($|t_{electron} - t_0|$) and ΔZ is the absolute value of the difference between the reported track initial z position and the vertex z position ($|z_{electron} - z_0|$). A cursory glance at these variables shows evidence for the need of more detailed timing calibrations but that a reasonable match requirement of $|\Delta T| < 1.8$ ns and $|\Delta Z| < 3.0$ cm will be almost fully efficient and produce a small amount of bias. Since there are skews and non-centered mean time effects, we will calibrate and then reselect to minimize this bias. We note that the z distribution looks well matched so we do not consider it further.

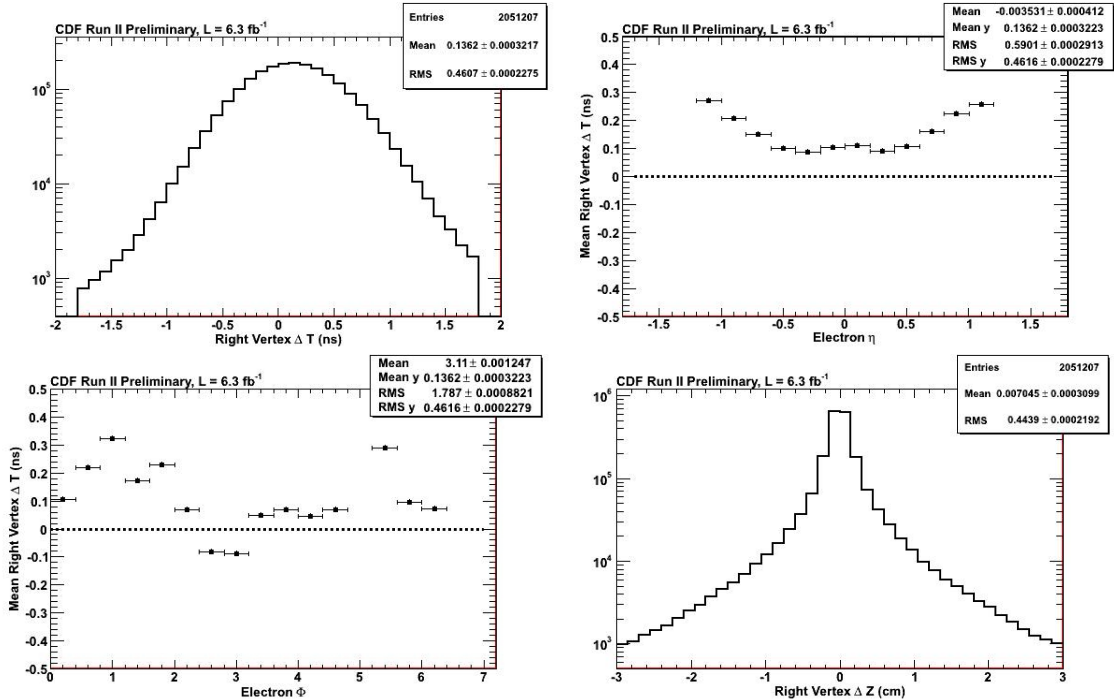


Fig. 3.3. The ΔT between the electron track and the vertex, ΔT vs. electron η , ΔT vs. electron ϕ , and the ΔZ between the electron track and the vertex before calibrations. Note that they are not centered at zero, demonstrating the need for further timing calibrations. Note that despite the timing bias, these figures show that the required matching requirements, listed in Table 3.1, are very efficient.

The first place to begin when calibrating the detector is with the calibration of COT tracks. These tracks acquire their timing information based on reconstructed hit times in the COT. The initial calibration of the COT times is described in Reference [71]. Our final calibration, described in Section 3.2, is designed to calibrate the t_0 of the tracks so that their timing variation as a function of any important variables is small compared to the individual track resolution which is ~ 0.4 ns.

Before describing the calibration it is worth describing the limiting terms in the track timing uncertainty as well as its overall resolution. For each track the tracking algorithms determines t_0 along with an uncertainty on the measurement of t_0 . This value, which we call $T_0\sigma$, is shown in Figure 3.4 for the good tracks in our sample that pass the requirements in Table 2.6. It is dominated by the ability to reconstruct tracks in a complicated environment where each hit is measured with a 1 ns TDC. This reported uncertainty is compared with a second measure that comes from vertices reconstructed from tracks. On the RHS of Figure 3.4 we see the RMS of the t_0 of the tracks fit to determine the mean time and z of the SpaceTime vertices matched to electrons. Both results are around ~ 0.5 ns, indicating that the $T_0\sigma$ of the tracks is likely a low end approximation. This implies that any systematic variations which are under the uncertainty of the measurement of the track itself will not significantly contribute to the systematic variation in t_{corr} which uses the vertices which combine the results from multiple tracks. Since we will get multiple measurements of approximately 0.5 ns resolution tracks, and the final t_{corr} resolution is dominated by the single 0.5 ns EMTiming measurement of t_f there is no significant value to improving the resolution of the tracks. Thus we begin the calibration procedure described in Section 3.2 by focusing on the variations in t_0 as a function of a number of important variables and calibrate these variations in each to make sure the biases are small compared to the resolution.

While this will make better measurements, we note that as the track time changes and the vertex time changes after calibrations, this has the possibility of making

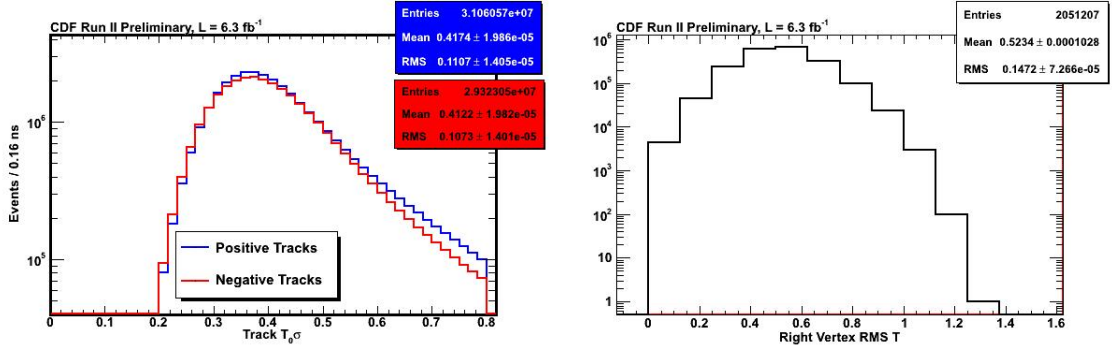


Fig. 3.4. (LHS) The reported $T_0\sigma$ for COT tracks (Blue = positively charged tracks and Red = negatively charged tracks) and (RHS) RMS of the t_0 of the tracks used in the vertex distributions. The track $T_0\sigma$ as well as the RMS of the tracks around the mean of the best fit vertex allow us to infer the intrinsic uncertainty of the timing measurement associated with the tracks and allow us to infer the necessary sensitivity of the calibrations of the track times.

individual events just pass or fail the selection requirements of the matching. To keep the timing distributions fully symmetric, and allows us to calculate the mean of the distribution rather than do a full fit, we reselect our data sample. As such, we proceed with a consistent set of events and then check for any remaining variations after corrections and proceed to remove any systematic variation. Once the tracks t_0 has been calibrated, we move to the calibration of the vertices. This begins by reselecting the $e+\cancel{E}_T$ sample using calibrated tracks in the SpaceTime vertex algorithm [63], as detailed in Section 3.3. After calibration of the tracks the vertexing can do a better job of combining tracks and give a better overall measurement of the collision position and time.

After calibrating the tracks and the vertices we reselect the $e+\cancel{E}_T$ sample again and turn to calibrating the arrival time as recorded by the EMTiming system. A proper calibration of the EMTiming system ensures accurate measurement of the arrival time of objects in the calorimeter while avoiding artificial biases due to event topology. The details of calibration of the EMTiming system is given in Section 3.4.

We note that the RMS of the EMTiming measurement is approximately 0.5 ns, but what we are interested in is whether there is a bias in the mean of the distribution as a function of any important variable, any of which can be calibrated out.

The summary of the full calibration procedure used to calibrate the COT, vertexing, and EMTiming systems for this analysis is summarized in Table 3.2 and briefly goes as:

Calibration Procedure Summary
Select a sample of $W \rightarrow e\nu$ events with a well-matched electron to a vertex
Select and calibrate a set of “good” COT tracks. If the calibration change is significant compared to the tolerances defined, reselect $W \rightarrow e\nu$ events and repeat this step
(Re)Select and calibrate a set of “good” SpaceTime vertices. If the calibration change is significant compared to the tolerances defined, reselect $W \rightarrow e\nu$ events and repeat this step
(Re)Select and calibrate the EMTiming system for well matched electron candidates in the calorimeter. If the calibration change is significant compared to the tolerances defined, repeat this step

Table 3.2

Table summarizing the calibration procedure for tracks, SpaceTime vertices, and EMTiming times. Each step in this procedure is iterated until the samples stabilize in terms of the magnitude of the corrections being generated and the track t_0 , vertex t_0 , and t_{corr} timing distributions fall within the tolerances defined for each.

- **Select a sample of $W \rightarrow e\nu$ events:**

Here we use the selection requirements outlined in Table 3.1 to select a sample of $W \rightarrow e\nu$ events corresponding to 6.3 fb^{-1} of data. Note that after each step in which the timing information is calibrated we will reselect our sample using all selection and matching criteria.

- **Select and calibrate a set of “good” COT tracks:**

For each event we select a set of tracks from our events using the track requirement in Table 2.6 in order to insure that we have good t_0 and z_0 measurements associated with each track. We then use a set of variables that have a strong impact on the track t_0 and fit the data using polynomials as well as cross terms in order to create track-by-track corrections which are then applied run-by-run. The variables and procedure is described in more detail in the Section 3.2. Using these corrected tracks we re-run the vertexing and reselect our $e+~~E~~_T$ sample using the calibrated track times. We iterate on this step until we find that the track corrections are less than 0.4 ns.

- **Calibrate “good” SpaceTime vertices:**

After the vertexing has been performed we select “good” SpaceTime vertices as defined in Table 2.10 and re-select events that have a well matched electron to the vertex. We next study these vertices to see if there is any variation as a function of any important variables. We note a bias in the overall vertexing measurement and, at this stage, calibrate this out (described in Section 3.3) on a run-by-run basis. Using these corrected vertices we reselect our $e+~~E~~_T$ sample. We iterate on this step until we find that the vertex timing corrections are less than 0.01 ns.

- **Calibrate the EMTiming System:**

After vertexing calibrations are done we reselect events and calculate t_{corr} for each electron so that we can calibrate the EMTiming system. In a manner similar to that of tracks, we find that the mean of the t_{corr} varies significantly as a function of many variables (described further in Section 3.4). We iterate on this step until we find that the EMTiming time corrections are less than 0.1 ns.

In the next sections give more detail about the individual procedures for COT Tracks, SpaceTime Vertices, and the EMTiming system. Finally, we present the results of all these individual calibrations on the t_{corr} variable and demonstrate that we have removed systematic variations as a function of all the important event observables to less than <100 ps.

3.2 Calibrating COT Tracks

In this section we detail the procedure for calibrating “good” COT tracks for use in the SpaceTime vertexing. Figure 3.5 shows the 1-dimensional timing distribution of t_0 of the tracks, after first event selection but before calibrations, as well as $\langle t_0 \rangle$ as a function of the various tracking variables. The five tracking parameters ($T_0\sigma$, ϕ , η , d_0 , and q) are chosen here because they uniquely describe the 3-dimensional track trajectory with the exception of Z along the beamline (this is expected to not have a mean of zero for reasons described in References [38,63,74] resulting from the structure of the beam and thus should not be calibrated against). Additionally, “Run Number” is used to account for any variation over time and data taking configuration. Clearly, positive and negative charge appear very different and there is significant variation in the mean time as a function of many of the variables. Not only is $\langle t_0 \rangle$ not centered at 0 ns, but there are systematic variations on the order of 1 ns. Additionally, these variations change independently over time (as a function of run number) as well as becoming increasingly worse for low p_T tracks. This is especially troublesome for the exclusive $\gamma+\cancel{E}_T$ analysis since we explicitly veto any event that has large p_T tracks, thus most of our vertices are made up of these poorly calibrated tracks.

Figure 3.6 shows how these poorly calibrated tracks effect even our selection of $e+\cancel{E}_T$ events by looking at the individual electron track time variables before calibrations. We draw attention to the fact that the electron track mean time is

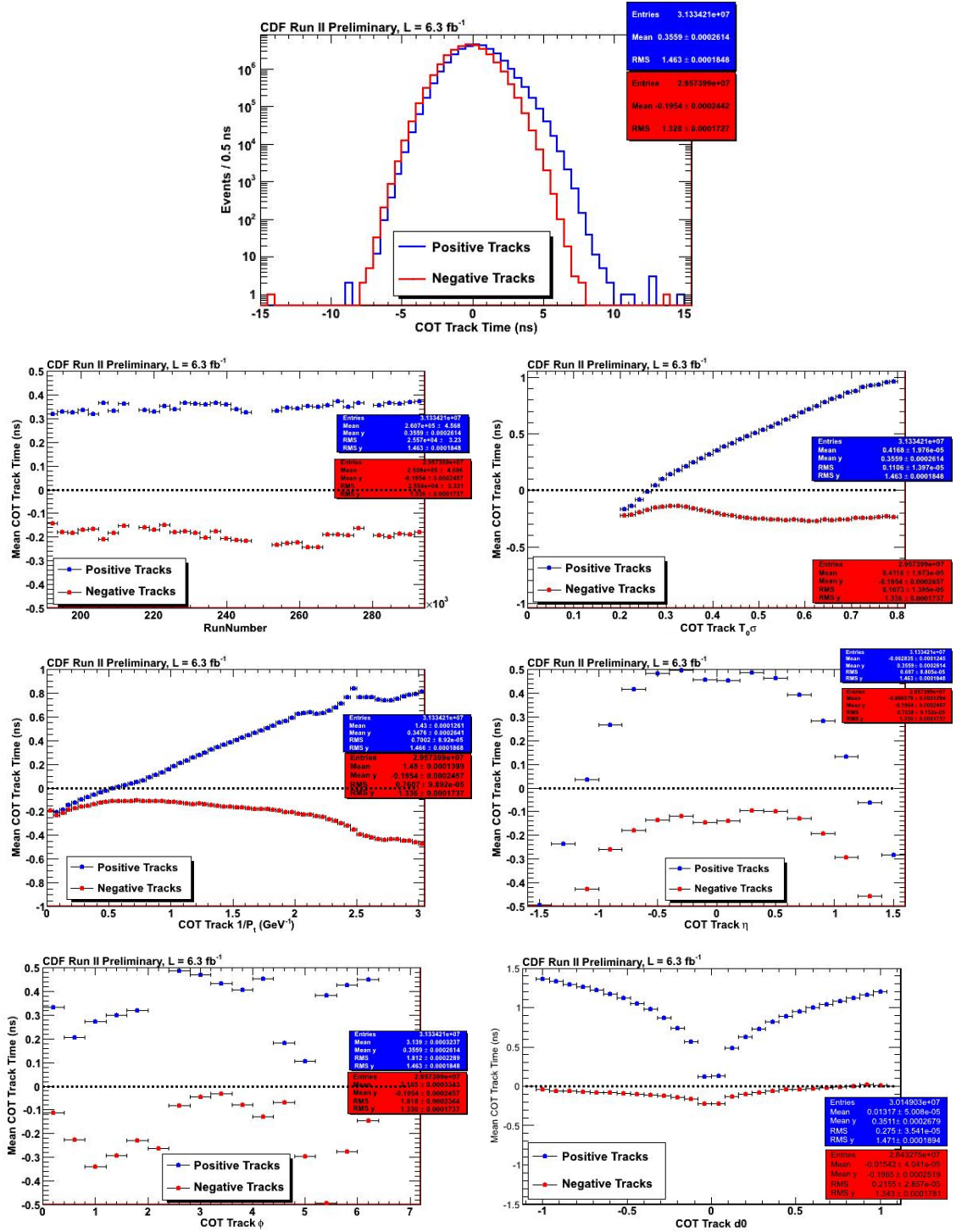


Fig. 3.5. The COT track t_0 for positive (blue) and negative charges (red) in the top row and the mean time of the COT tracks, $\langle t_0 \rangle$, plotted as a function of various variables before calibrations. Note the scale on the y-axis in some of the plots is much larger than others.

not well centered at $t_0 = 0$ and there is a large systematic variation in $\langle t_0 \rangle$ as a function of η , ϕ , and run number.

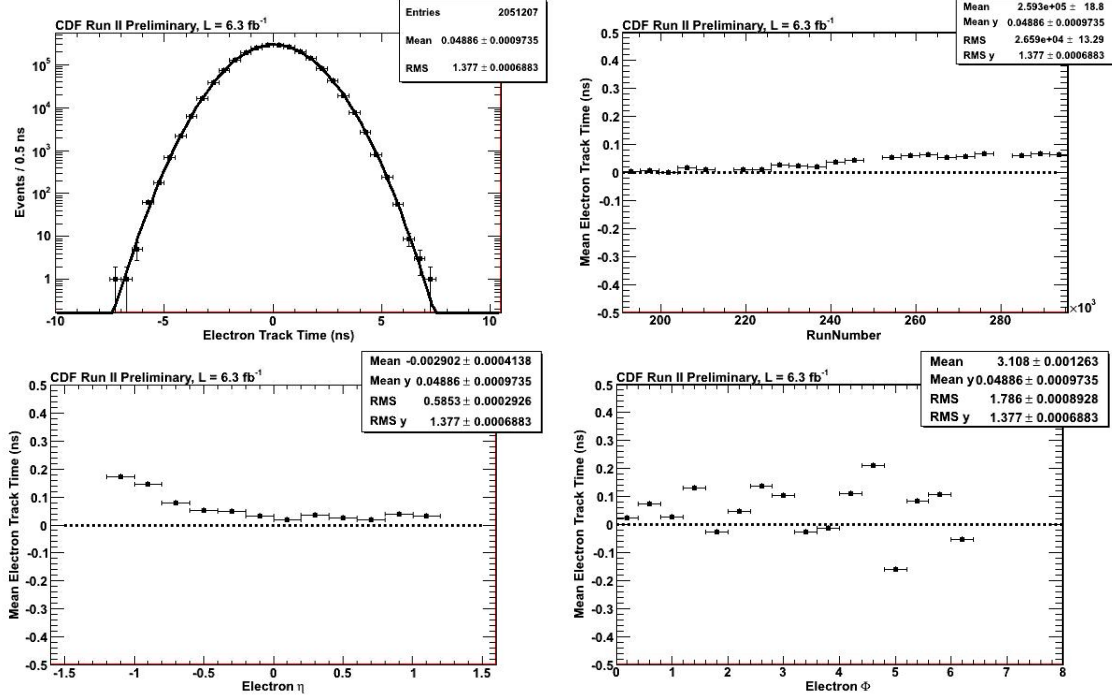


Fig. 3.6. The electron track t_0 , and mean t_0 as a function of Run-Number η and ϕ variables before calibrations.

As described previously, we begin the calibration procedure with the goal to calibrate the t_0 of the tracks such that the systematic variation small compared to the intrinsic resolution of the track itself of 0.4 ns. Table 3.3 gives the summary of the track calibration procedure, a more detailed description follows:

- **Select $W \rightarrow e\nu$ candidate events:**

Select $W \rightarrow e\nu$ candidate events where the electron track is well matched to any good SpaceTime vertex (see Table 3.1).

- **Calibrate the timing versus variables that have an impact on the track time:**

COT Track Calibration Procedure Summary
Select $W \rightarrow e\nu$ candidate events
Determine the mean track time, $\langle t_0 \rangle$, as a function of important variables and use this as a timing correction to make the $\langle t_0 \rangle = 0$ ns as a function of all variables. (Run Number, $T_0\sigma$, ϕ , η , d_0 , and q)
Reselect $W \rightarrow e\nu$ candidate events and iterate until the corrections converge

Table 3.3

Table outlining the COT track calibration procedure.

Determine the $\langle t_0 \rangle$ as a function of Run Number, $T_0\sigma$, Φ , η , Impact Parameter (d_0), and q , where each variable is described in Appendix B.1. The calibration procedure is to perform a polynomial fit of the timing distribution as a function of these variables, taking into account correlations from their cross-terms as many variables are highly correlated in the original tracking fit procedure. We then take these fits as corrections to the track times to center each at $\langle t_0 \rangle = 0$ ns.

- **Reselect $W \rightarrow e\nu$ candidate events:**

Re-select $W \rightarrow e\nu$ candidate events using the generated calibrations including re-running the vertexing. We continue to iterate this procedure until the largest deviation in the fit as a function of any variable is less than 0.4 ns.

Figure 3.7 shows $\langle t_0 \rangle$ as a function of the 1-d variables after applying the calibrations and iterating multiple times. We note that for the calibrated COT tracks there is no longer any significant difference between positive and negative tracks as was seen before the calibrations. Additional studies show that the tracks are well calibrated in two dimensional profile plots as well [75]. Furthermore, the systematic variations of the track t_0 are all well within the 0.4 ns tolerances versus the dominant variables. It is important to draw attention to the fact that the range

of the y-axis in the plots before calibrations (Figure 3.5) was large, ranging from -1.5 ns to 1.5 ns while the range shown after calibration (Figure 3.7) is now -0.5 ns to 0.5 ns. Thus, the structure that is visually present in Figure 3.7 is significantly exaggerated when compared to the plots before calibrations.

A second check, shown in Figure 3.8, shows the effect these track calibrations have on the electron track time showing that much of the variation is now gone, despite the fact that some residual variation in ϕ remains. This variation in ϕ is well within the individual track resolution and is thus not considered a problem for vertexing.

3.3 Verticies

Once the tracks t_0 have been calibrated using the procedure described in the previous section, we move to the calibration of the vertexing. Since the measurement of the initial time of the event, t_0 in Equation 1.8, is directly extracted from the vertex time information, this is a particularly important quantity to have calibrated as accurately as possible. Thus, we define our tolerance for systematic variation in the vertex calibration to be <0.1 ns.

We begin the calibration of the SpaceTime vertices by re-selecting our sample of $W \rightarrow e\nu$ candidate events using the calibrated tracks and re-running the SpaceTime vertexing algorithms. The vertex timing distribution after track calibrations, but before any additional vertex calibrations, can be seen in Figure 3.9. We see that there is still a systematic shift in the vertex mean time. This likely results from the fact that the SpaceTime vertex algorithm only selects a subsample of all the tracks in the event; the remaining tracks are unrelated and can cause biases in the overall tracking calibration that is fixed by the vertexing procedure of combining multiple tracks to eliminate bias. As a result any bias in the selection of tracks used in the tracking calibrations algorithm may introduce a slight offset in the mean time and thus need to be corrected for. We note that this effect is small, only has a shift of

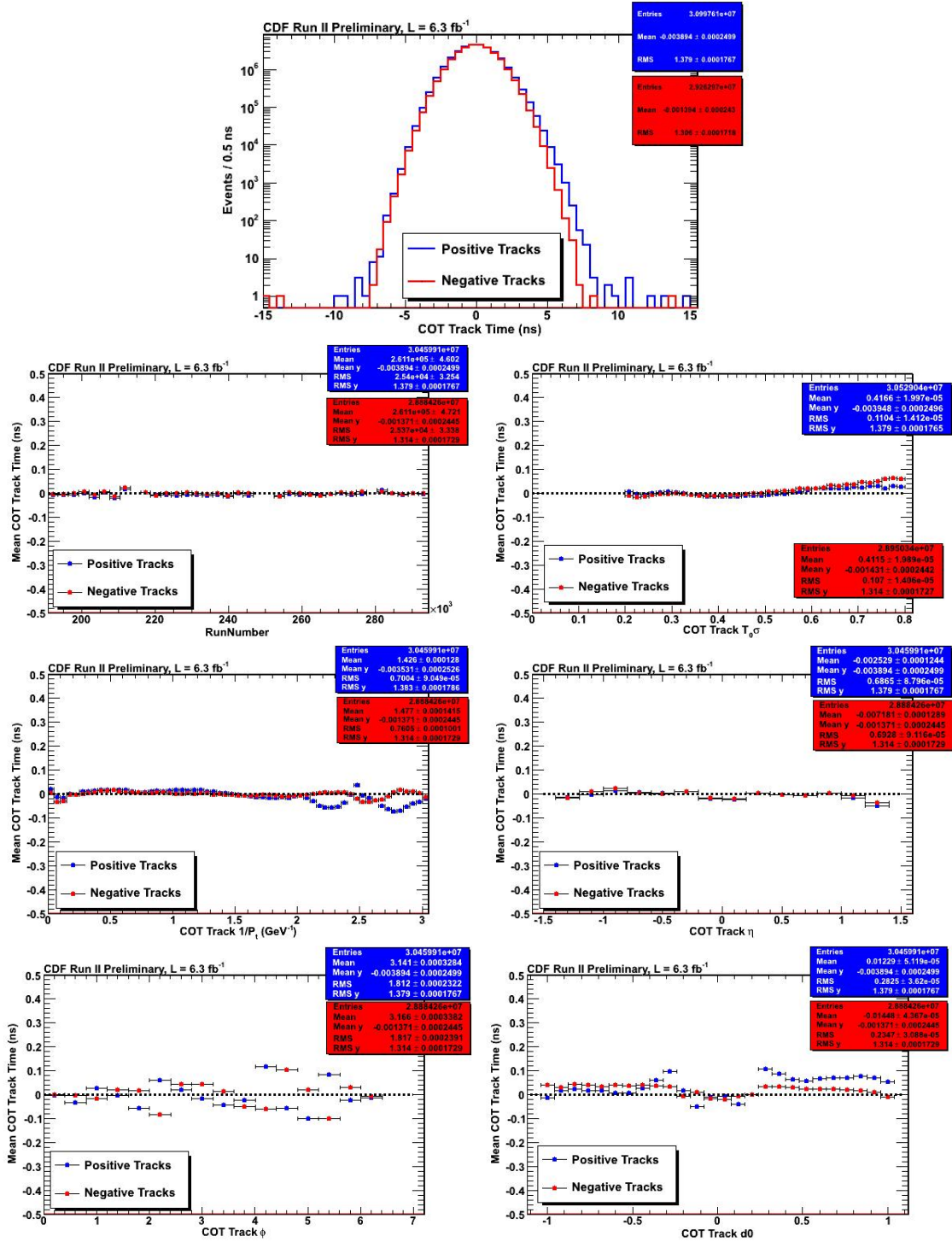


Fig. 3.7. The COT track t_0 after calibrations for positive (blue) and negative charges (red) in the top row and the mean time of the COT tracks, $\langle t_0 \rangle$, plotted as a function of various variables. Note the scale on the y-axis is now ± 500 ps.

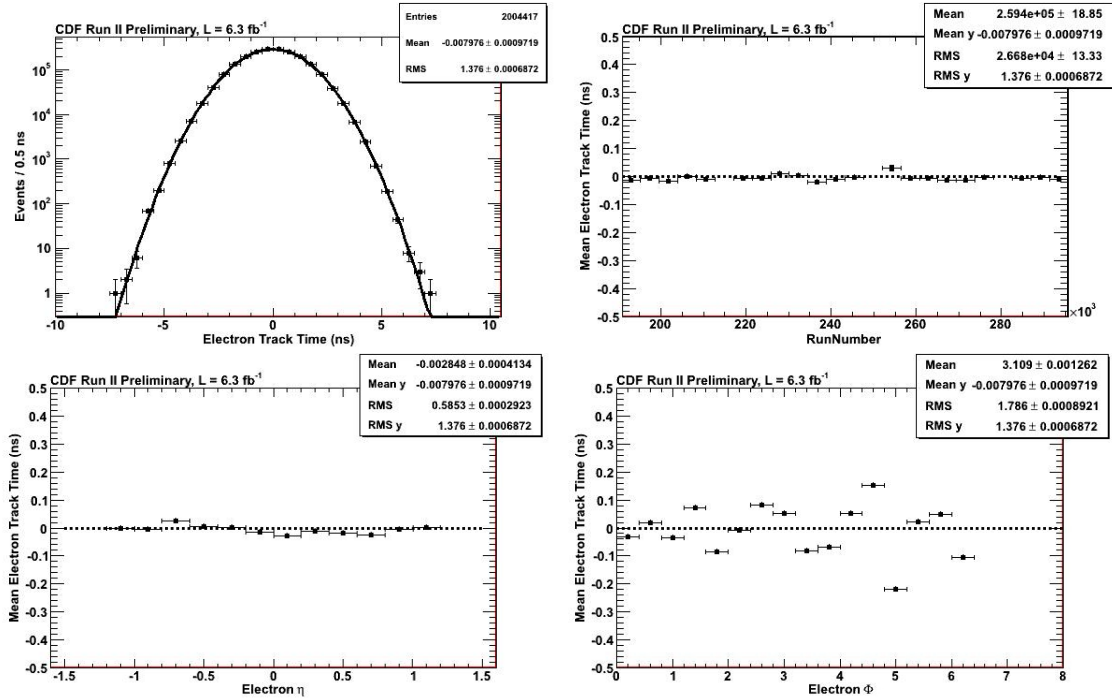


Fig. 3.8. The electron track t_0 , and $\langle t_0 \rangle$ as a function of Run-Number η and ϕ variables after calibrations. Note the variations are small here compared to the variations in Figure 3.6.

~ 55 ps. However, we have more than enough statistics to determine this mean to high precision and thus can remove this offset. This time we show that the $\langle t_0 \rangle$ versus z position in Figure 3.9 and again note that has a prevalent slope. The plot of the mean vertex time versus ΣP_T in Figure 3.9 is believed to have an offset reflecting the offset in Run Number. As we will see this variation vanishes after calibrations are applied. We describe the vertex timing calibration procedure, which is summarized in Table 3.4, below.

- **Reselect $W \rightarrow e\nu$ candidate events:**

Reselect $W \rightarrow e\nu$ candidate events, using calibrated tracks, where the electron track is well matched to a good SpaceTime Vertex (See Table 3.1).

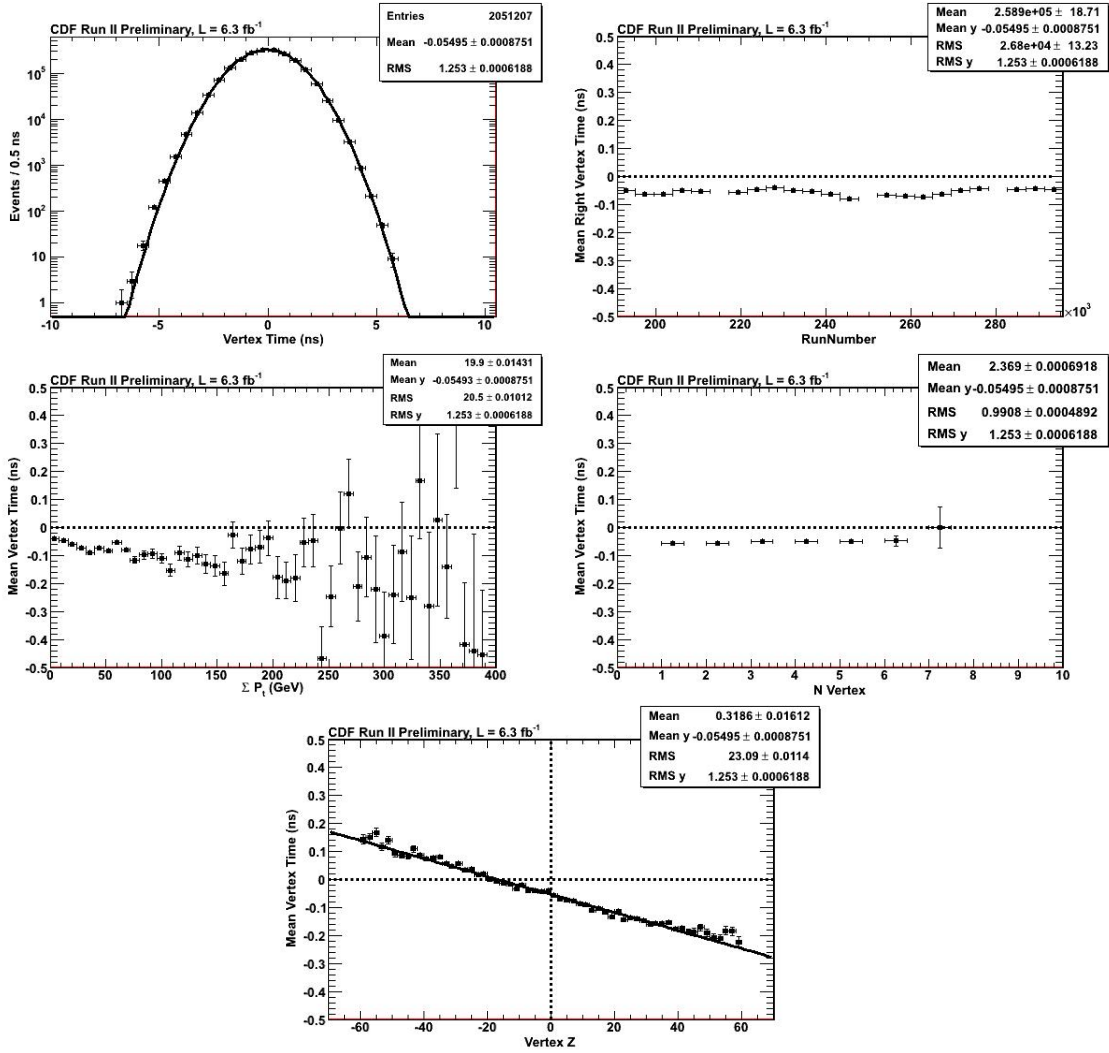


Fig. 3.9. The SpaceTime vertex t_0 as well as $\langle t_0 \rangle$ plotted versus various variables after track calibrations, but before vertex calibrations. This demonstrates that even following the COT track calibrations there is still a systematic offset of the mean time on the order of 55 ps, thus necessitating a simple calibration subtraction. The slope in the bottom figure of $\langle t_0 \rangle$ vs. z is expected and described in detail in Reference [74].

- Calibrate the vertex time versus variables that have an impact on the vertex time:

Vertex Calibration Procedure Summary
Reselect $W \rightarrow e\nu$ candidate events
Determine the mean vertex time, $\langle t_0 \rangle$, as a function of important variables and use this as a timing correction to make the average $\langle t_0 \rangle = 0$ as a function of all variables. (Run Number)
Reselect $W \rightarrow e\nu$ candidate events and iterate until the corrections converge

Table 3.4

Table outlining the SpaceTime vertex calibration procedure.

Determine $\langle t_0 \rangle$ of the vertex as a function of Run Number since this variable has the overall systematic shift in the mean time. Average all the times within the same run number and subtract off the difference from $\langle t_0 \rangle = 0$ in the average. Apply this generated correction to each vertex event-by-event.

- **Reselect $W \rightarrow e\nu$ candidate events and iterate:**

Reselect $W \rightarrow e\nu$ candidate events, using the vertex calibrations. We continue to iterate this procedure until the largest deviation in the mean is less than <0.01 ns per run.

The results of this calibration can be seen in Figure 3.10. Clearly, these corrections maintain the vertex time distribution to be Gaussian to many sigma and well centered at $t_0 = 0$. Figure 3.10 also shows the $\langle t_0 \rangle$ versus other variables (vertex ΣP_T , number of vertices present in the event, vertex z position) in order to demonstrate that none of the calibrations have introduced any unforeseen biases. We have included the z distribution here for completeness. Specifically, the variation in ΣP_T has disappeared and the expected slope in $\langle t_0 \rangle$ vs. z plot remains. Finally, coming back to the issue raised at the beginning of this chapter, Figure 3.11 also shows that the COT track calibrations and the vertex calibration maintain their balance between the track times and the vertex times by plotting the ΔT and ΔZ between

the vertex and the electron track versus Run Number and showing them to be both well centered and flat over time.

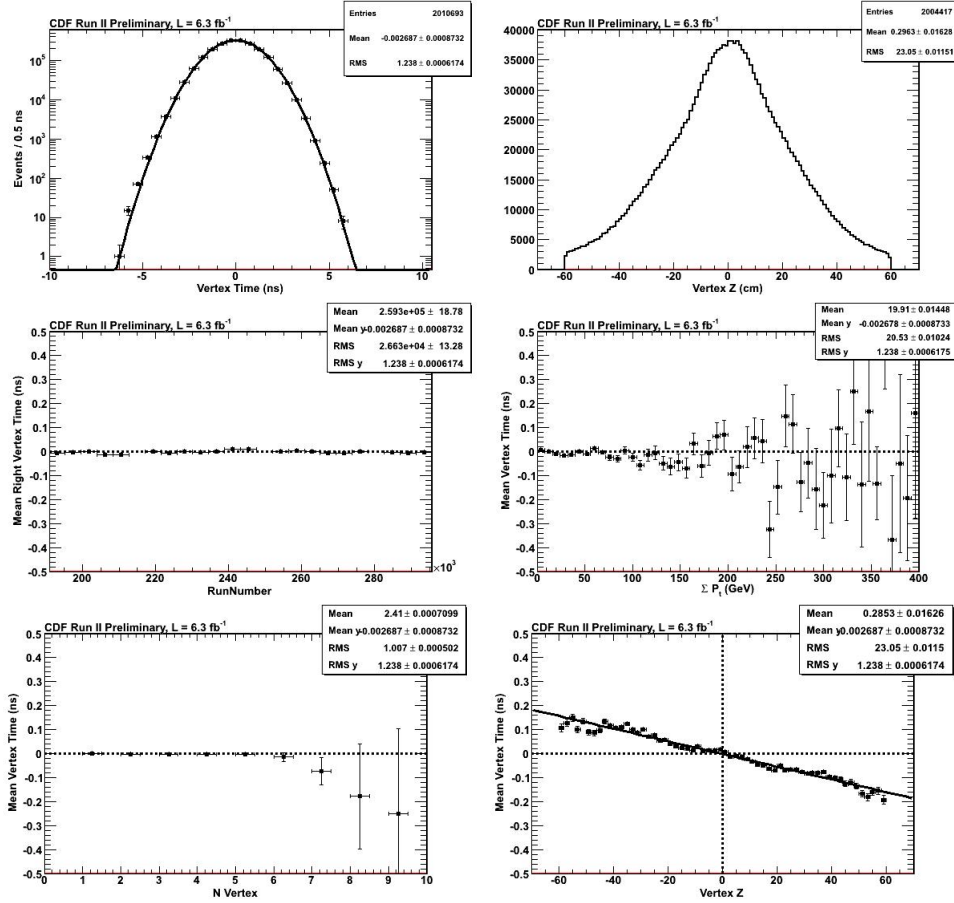


Fig. 3.10. The SpaceTime variables after calibrations showing that the vertexing is well calibrated. The slope in the bottom figure of mean $\langle t_0 \rangle$ vs. z is expected and described in detail in Reference [74].

With the vertexing well calibrated, we can move to calibrate the EMTiming system. In the next section we outline the procedure for calibrating the corrected time which takes into account the calibration of the EMTiming system as well as correlations between the EMTiming system and the COT, as well as event-by-event

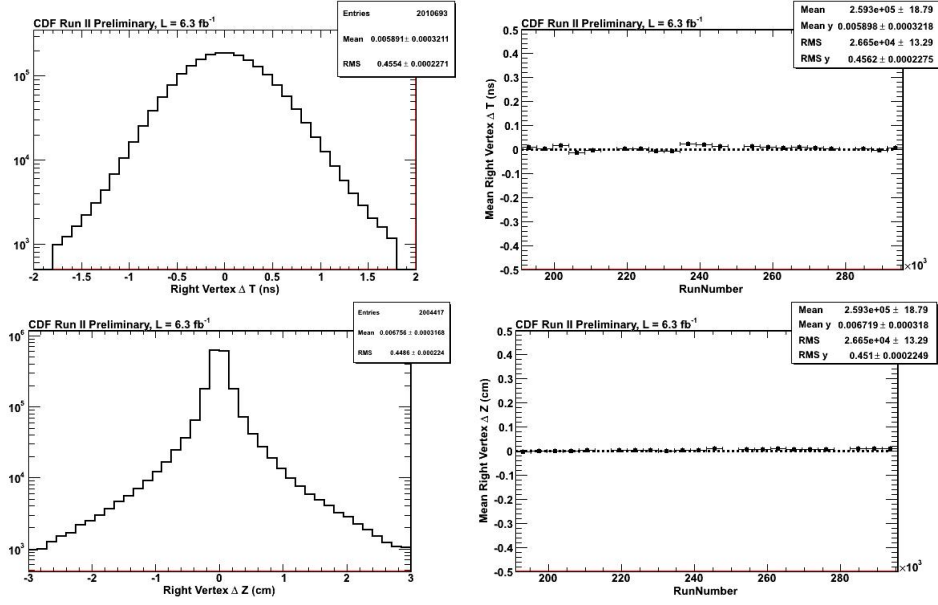


Fig. 3.11. (Top) The ΔT and (Bottom) ΔZ and $\langle \Delta T \rangle$ and $\langle \Delta Z \rangle$ vs Run Number between the electron track and the Space-Time vertex demonstrating that the track and vertex calibrations have removed any bias between the electron track and the Space-Time vertex.

corrections that occur because of different time-of-flight from the vertex to the CEM tower location.

3.4 EMTiming

In order to calibrate the EMTiming time associated with the well matched electrons one must take special care not to artificially calibrate against any real effects due to the underlying topology of the events selected and instead only calibrate out real systematics in the system. To do this we follow a calibration procedure that differs slightly from the methods used for tracks and vertices as well as by previous versions of this analysis. Previous calibrations (Reference [38]) simply calibrated

against the average EMTiming time or time corrected for the average time of flight. We now call this t_{corr}^0 and it is defined as

$$t_{corr}^0 = t_f - t_0 - \frac{|\vec{x}_f - \vec{x}_0|}{c} \quad (3.12)$$

where t_0 is equal to zero (the average time of collision in the center of the detector) and $x_0 = 0$ cm, which is the center of the detector. We will show why this is the wrong procedure and outline a more proper procedure that takes into account the best estimate of the vertex time and time-of-flight of the electron event-by-event.

To calibrate the EMTiming system we calibrate against the mean t_{corr} , $\langle t_{corr} \rangle$, as a function of variables that the EMTiming time should not have systematic variation with respect to. This is because the EMTiming system measures the time of arrival, not the time of collision. Thus, we want to make sure we are not biased by time-of-flight systematics from the sample we have chosen. For example, if most of the electrons that hit a tower at high $|\eta|$ are from a different average collision z_0 or t_0 than from low $|\eta|$, then they will be calibrated to different expected arrival times rather than to their true time-of-origin and time-of-flight. Said differently, we want to calibrate on the actual time-of-flight, not to average t_0 and z_0 positions that produce hits in this tower. We find that there are three variables of interest to calibrate in which the corrected time distribution shows significant variation. They are run number, energy, and tower number. These distributions are shown in Figure 3.12 and were chosen because they correspond to the physical location in the detector and exhibited the need for additional calibrations. While there are other interesting variables, such as z of the vertex, we will use them as a check of our methods.

After reselecting $W \rightarrow e\nu$ events where we match the electron to the SpaceTime vertex, using the calibrated tracks and vertices, we use the calibrations derived from the ‘uncalibrated’ t_{corr} distributions obtained from as the parent distributions for the EMTiming calibrations. The calibration procedure is outlined in Table 3.5 and described in more detail below.

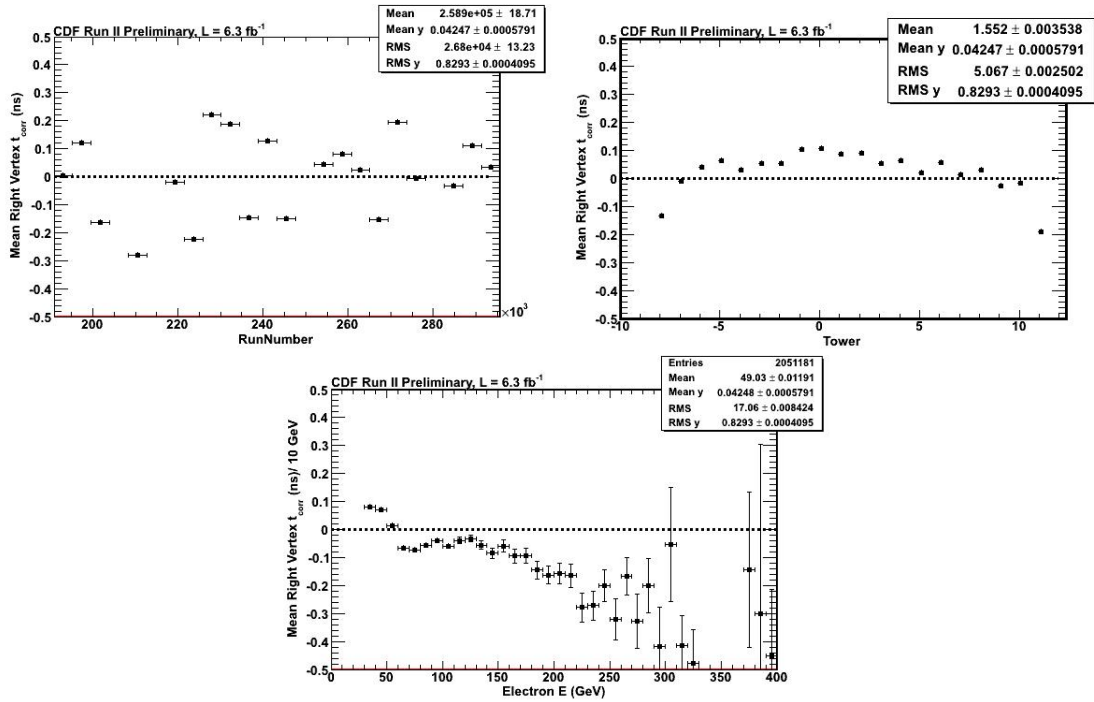


Fig. 3.12. The $\langle t_{corr} \rangle$ distributions before EMTiming calibrations used to generate the run-by-run, tower, and energy calibrations.

EMTiming Calibration Procedure Summary
Reselect $W \rightarrow e\nu$ candidate events
Determine the mean t_{corr} , $\langle t_{corr} \rangle$, as a function of important variables and use this as a timing correction to make the average $\langle t_{corr} \rangle = 0$ ns as a function of all variables (Run number, Tower, Energy)
Iterate until the corrections converge

Table 3.5

Table outlining the EMTiming time calibration procedure.

- Reselect $W \rightarrow e\nu$ candidate events:

Reselect the subset of $W \rightarrow e\nu$ candidate events where the electron track is well matched to a good SpaceTime Vertex (See Table 3.1). Note this step uses the previous track and vertex calibrations already performed.

- **Calibrate variables that have an impact on the corrected time:**

Determine $\langle t_{corr} \rangle$ as a function of: Run Number, tower, and energy. There should be no systematic dependencies on $\langle t_{corr} \rangle$ as a function of these variables. Create a set of corrections that make $\langle t_{corr} \rangle = 0$ ns as a function of Run Number, for each tower independently, and energy. We then apply this set of corrections to the EMTiming time.

- **Iterate this procedure until the calibrations reach convergence:**

We continue to iterate this procedure until the resulting variation in the calibration becomes less than 0.1 ns. Note, unlike before, it is unnecessary to reselect our sample. This is because the arrival time of the electrons that is being calibrated during this procedure does not effect the content of our sample.

Finally we present the result of the full set of timing calibrations, including the EMTiming calibrations described here.

3.5 Summary and Validation Results

The results for the entire calibration procedure are shown in Figure 3.13 using t_{corr} for electrons that are well-matched to a vertex. The resulting t_{corr} distribution has a mean of 0.002 ns and an RMS of 0.69 ns, which is well within the nominal expectations of having a mean of 0.0 ns and an RMS of 0.65 ns. We also see in Figure 3.13 that the $\langle t_{corr} \rangle$ distribution is flat and centered as a function of other variables that were not part of the calibration procedure including vertex ΣP_T , vertex z , and number of vertices in the event. The fact that the distributions are flat versus important variables that we should not calibrate on, especially the z of the

collision, gives us confidence that we have taken into account all important sources of calibration bias. We also see that none of these distributions have a systematic variation >0.1 ns thus placing us well within our predefined tolerances for our timing measurement. Finally, we note that the timing distribution is Gaussian out to many sigma. It is possible that the events on the tail are due to non-collision events such as cosmic rays, but this has not been studied in further detail as it has no impact on our conclusions about how well the detector is calibrated.

Before we conclude this chapter we make a few comments about the differences between calibrating on t_{corr} versus the old method of calibrating on t_{corr}^0 . We show the EMTiming time (t_{corr}^0) distributions after all calibrations in Figure 3.13. It is evident that this calibration did have the desired effect for most, but not all variables. For the t_{corr}^0 for well-matched electrons we observe that the distribution is Gaussian out to many sigma and has a mean of 0.05 ns. The t_{corr}^0 distribution is also very flat with little variation over the entire run range as well as having no geometric variation by tower (η), ϕ , or z position (z CES position). However, the last plot in Figure 3.14 shows a timing shift of ~ 200 ps starting at 50 GeV for t_{corr}^0 which is not seen in Figure 3.13. This shift can be understood as being a real effect due to detector and reconstruction properties of the sample of events being examined and thus does not offer concern to the calibration of the final sample using our method. This becomes evident when we look at the time-of-flight (TOF) from the right vertex as a function of energy and tower shown in Figure 3.15.

Now that we have confirmed that our detector is well calibrated and free of timing biases, we turn our attention to the sources of background in the exclusive $\gamma_{delayed} + \cancel{E}_T$ final state. In the next chapter we address non-collision sources of backgrounds and lay out a series of selection requirements to reduce their present in our final state.

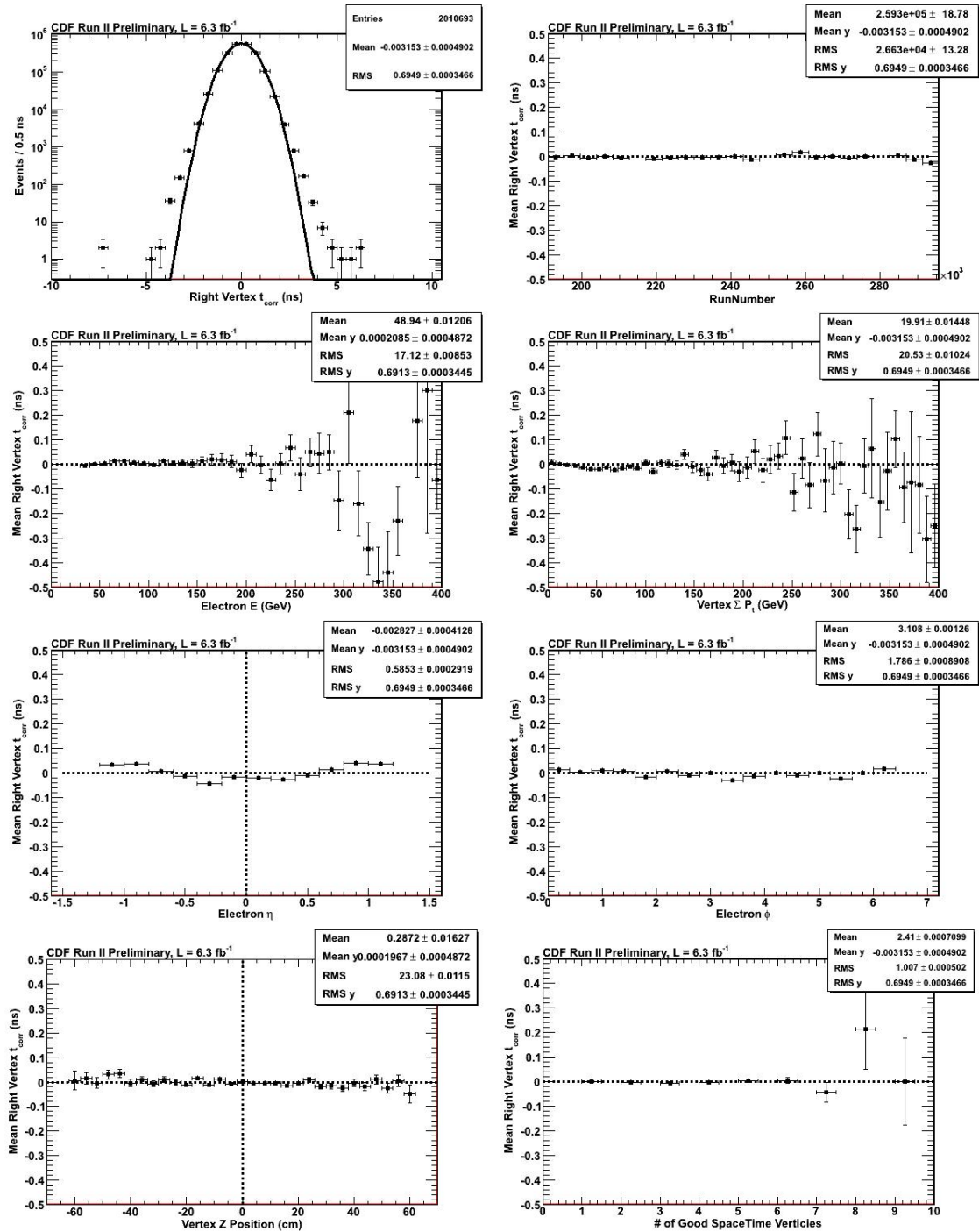


Fig. 3.13. The distribution of t_{corr} after the full set of calibrations for the $W \rightarrow e\nu$ sample. We note that the distributions have a mean of 0.002 ns and an RMS of 0.69 ns, which is well within the nominal expectations of having a mean of 0.0 ns and an RMS of 0.65 ns. We also see that the distribution of $\langle t_{corr} \rangle$ is flat and centered as a function of run number, energy, vertex ΣP_T , η , ϕ , vertex z , and number of vertices in the event.

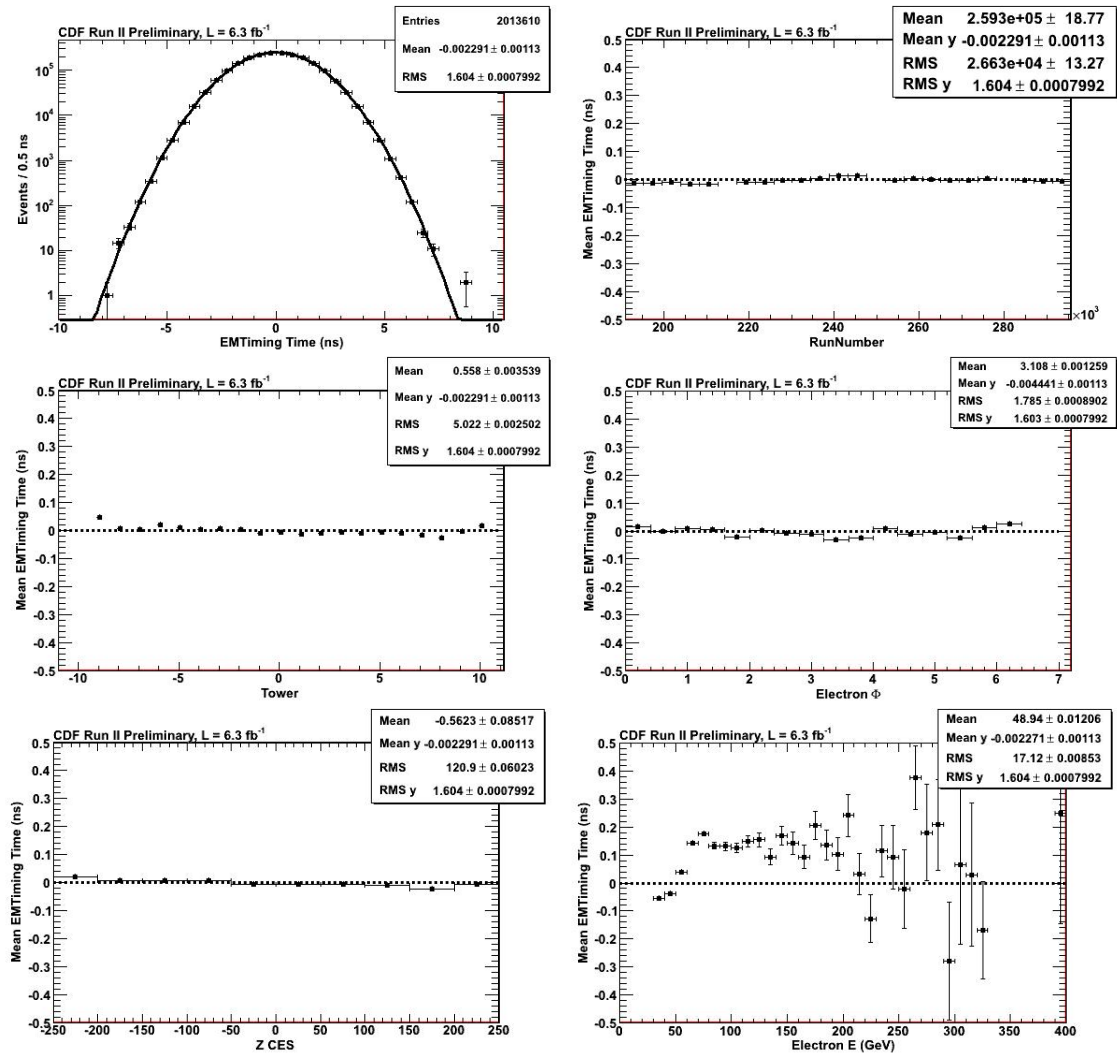


Fig. 3.14. EMTiming variables, t_{corr}^0 , after calibrations. Note that this variable is not flat as a function E .

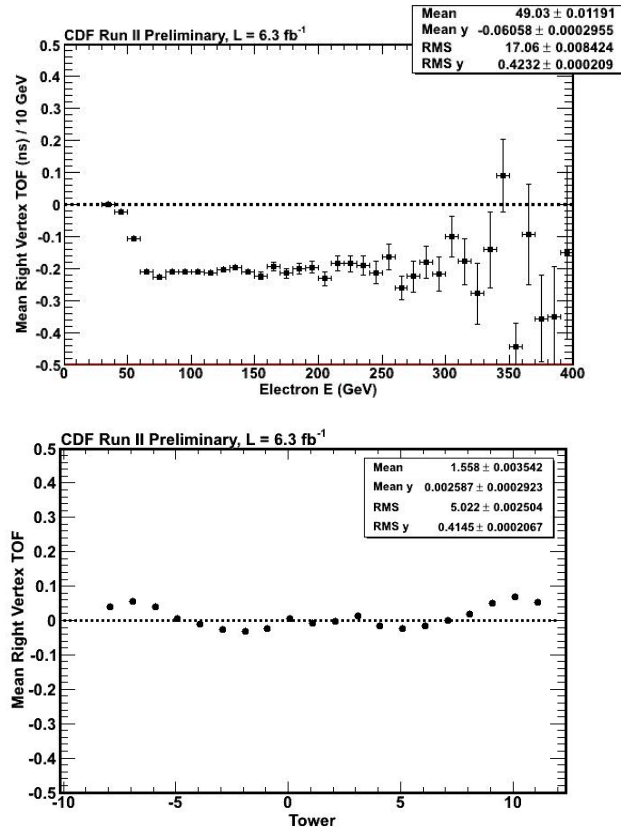


Fig. 3.15. The mean time-of-flight correction from the right vertex, instead of $z = 0$ cm, as a function of energy and tower after calibrations for the $W \rightarrow e\nu$ sample. The evidence of variation in this variable gives us an understanding of why calibrating versus t_{CORR}^0 does not take into account the effect due to detector and reconstruction properties of the sample of events.